HHS Public Access

Author manuscript

Biomaterials. Author manuscript; available in PMC 2017 July 01.

Published in final edited form as:

Biomaterials. 2016 July ; 93: 27–37. doi:10.1016/j.biomaterials.2016.03.021.

Differential Regulation of Angiogenesis using Degradable VEGF-Binding Microspheres

David G. Belair[1], **Michael J. Miller**[2], **Shoujian Wang**[3], **Soesiawati R. Darjatmokon**[3], **Bernard Y.K. Binder**[4], **Nader Sheibani**[1,3], and **William L. Murphy**[1,5,6,*]

[1]Department of Biomedical Engineering, University of Wisconsin-Madison

[2]Department of Chemical and Biological Engineering, University of Wisconsin-Madison

[3]Department of Ophthalmology and Visual Sciences, University of Wisconsin-Madison

[4]Department of Surgery, University of Wisconsin-Madison

[5]Material Science Program, University of Wisconsin-Madison

[6]Department of Orthopedics and Rehabilitation, University of Wisconsin-Madison

Abstract

Vascular endothelial growth factor (VEGF) spatial and temporal activity must be tightly controlled during angiogenesis to form perfusable vasculature in a healing wound. The native extracellular matrix (ECM) regulates growth factor activity locally *via* sequestering, and researchers have used ECM-mimicking approaches to regulate the activity of VEGF in cell culture and *in vivo*. However, the impact of dynamic, affinity-mediated growth factor sequestering has not been explored in detail with biomaterials. Here, we sought to modulate VEGF activity dynamically over time using poly(ethylene glycol) microspheres containing VEGF-binding peptides (VBPs) and exhibiting varying degradation rates. The degradation rate of VBP microspheres conferred a differential ability to up- or down-regulate VEGF activity in culture with primary human endothelial cells. VBP microspheres with fast-degrading crosslinks reduced VEGF activity and signaling, while VBP microspheres with no inherent degradability sequestered and promoted VEGF activity in culture with endothelial cells. VBP microspheres with degradable crosslinks significantly reduced neovascularization *in vivo*, but neither non-degradable VBP microspheres nor bolus delivery of soluble VBP reduced neovascularization. The covalent incorporation of VBP to degradable microspheres was required to reduce neovascularization in a mouse model of choroidal neovascularization *in vivo*, which demonstrates a potential clinical application of degradable VBP microspheres to reduce pathological angiogenesis. The results herein highlight the ability to modulate the activity of a sequestered growth factor by changing the crosslinker identity within PEG hydrogel microspheres. The insights gained here may instruct the design and translation of affinity-based growth factor sequestering biomaterials for regenerative medicine applications.

*Corresponding author, William L. Murphy, can be contacted at Wisconsin Institute for Medical Research, 1111 Highland Avenue Room 5405, Madison, WI 53705. Phone: (608)262-2224. correspondence: wlmurphy@wisc.edu.

Keywords

Degradable biomaterials; vascular endothelial growth factor; growth factor sequestering; biomimetic microspheres; endothelial cells; choroidal neovascularization

Introduction

Endothelial cell function during angiogenesis requires control over vascular endothelial growth factor (VEGF) activity [1]. VEGF must be maintained in a limited concentration range to initiate angiogenesis during wound healing and ultimately to form patent new vasculature [2,3]. Unregulated VEGF expression often results in hemangioma formation *in vivo* [4,5], and high levels of VEGF activity promote aberrant angiogenesis associated with poor musculoskeletal wound healing [6,7] and diseases including telangiectasia [8], tumor growth [9], retinopathy [10], and choroidal neovascularization [11,12]. The native extracellular matrix (ECM) modulates the cell response to VEGF, and synthetic biomaterials designed to mimic the ECM can regulate VEGF activity in culture and *in vivo* [13,14]. For example, VEGF loaded hydrogels containing heparin binding peptide amphiphiles potentiated VEGF signaling in culture and *in vivo* [15–18], and VEGF loaded hydrogels containing fibronectin-mimicking peptides increased VEGF-dependent EC function *in vitro* and increased neovascularization *in vivo* [19]. However, fibronectin and heparin can promiscuously bind multiple growth factors [20–22], and are thus limited in their ability to regulate VEGF with specificity. Our group previously developed synthetic microspheres that specifically modulated VEGF activity in culture using pendant VEGF-binding peptides (VBPs) designed to mimic VEGF receptor 2 (VEGFR2) [23–26]. VBP microspheres specifically sequestered VEGF in serum-containing medium, reduced endothelial cell proliferation upon VEGF sequestering in culture [24,25], and stimulated endothelial cell proliferation via sustained release of active VEGF [23,25]. However, the influence of biomaterial degradation on affinity-mediated VEGF regulation has not been explored in detail. Given the importance of VEGF temporal regulation during angiogenesis, we sought to design biomaterials capable of highly specific VEGF sequestering and with a tunable degradation rate.

VEGF activity is temporally regulated during natural wound healing, as VEGF promotes endothelial cell (EC) proliferation and sprouting during early angiogenesis (days 1–7)[27], and VEGF dependence is reduced during days 7–14 [28]. We sought to design injectable, degradable VBP microspheres with crosslinking groups of varying degradability to limit VEGF regulation to an early time window [29,30]. We hypothesized that VBP microsphere degradation would dynamically regulate VEGF activity over time *in vitro* and modulate VEGF-dependent vascular growth in a model of choroidal neovascularization *in vivo*. Results here show that fast-degrading VBP microspheres (F-VBP microspheres) reduced VEGF signaling and activity in both two-dimensional EC culture and in a three-dimensional endothelial sprouting assay, while non-degrading VBP microspheres (N-VBP microspheres) increased VEGF signaling and activity in culture upon VEGF release. F-VBP microspheres also reduced mouse choroidal neovascularization *in vivo* while N-VBP had no effect on

neovascularization. This study demonstrates that degradable, growth factor-binding biomaterials enable differential regulation of growth factor activity *in vitro* and *in vivo*.

Materials and Methods

Peptide synthesis and characterization

Peptides were synthesized and characterized as previously described [23]. VEGF-binding peptide (VBP) and a peptide with the same composition as VBP but with a scrambled sequence (Scramble) were synthesized using fmoc solid phase peptide synthesis on an automated microwave peptide synthesizer (Discover; CEM) equipped with automated liquid handling (Liberty1; CEM). All amino acids and Rink Amide MBHA resin were purchased from EMD Novabiochem. Resin was initially swelled in N,N-dimethylformamide (DMF; Fisher) for 10 minutes and subsequently deprotected in 20 vol.% piperidine (Sigma), 80 vol. % DMF, and 0.1M HOBt (Advanced Chem Tech) for 5 minutes under microwave at 70°C. Resin was washed twice in DMF before coupling, and the reaction vessel was subsequently filled with four molar equivalents of amino acid (dissolved at 0.2M in DMF) with respect to free amines, four equivalents of HBTU (Advanced Chem Tech), and eight equivalents of diisopropylethylamine (DIPEA; Fisher), which was dissolved at 35 vol.% in N-methyl-2-pyrrolidone (Fisher). Coupling for all amino acids was performed at 70°C (except for cysteine, which was coupled at 50°C) for 5 minutes under microwave. Peptide purity was verified using reverse phase high performance liquid chromatography (Shimadzu C_{18} column). Peptide identity was verified using time-of-flight mass spectroscopy (MALDI-ToF; Bruker), and peptide content was determined using an Ellman's assay (Thermo Scientific) to measure free thiols.

PEG derivatization with norbornene

Poly(ethylene glycol) (PEG; M_n = 20,000; Jenkem) with four or eight arms was derivatized with norbornene groups on each arm as previously described [23]. All reagents here were purchased from Sigma-Aldrich. Briefly, 4-arm PEG (terminated with hydroxyl groups) was reacted under inert gas with ten molar equivalents 5-norborne-2-carboxylic acid in dichloromethane, five molar equivalents N,N'-dicyclohexylcarbodiimide, half molar equivalent 4-diethylaminopyridine, and five molar equivalents of pyridine. Derivatized PEG was precipitated in ice cold diethyl ether (Fisher), dried, dialyzed against deionized (DI) water, and lyophilized. Four-arm and eight-arm PEG functionalization with norbornene was verified with ^{1}H nuclear magnetic resonance as described [31].

Synthesis of ester-containing PEG dithiol molecules

PEG-diester dithiol molecules were synthesized as described elsewhere [32] through the reaction of hydroxy-terminated PEG (M_n = 3,400; Spectrum) with thiol-containing molecules, 3-mercaptopropionic acid (MP Biomedicals) or thioglycolic acid (MP Biomedicals). PEG derivatized with 3-mercaptopropionic acid is hereafter referred to as PEG-M-DT, and PEG derivatized with thioglycolic acid is hereafter referred to as PEG-T-DT. PEG was dried *via* reflux in toluene under argon gas, and subsequently 3-mercaptopropionic acid or thioglycolic acid was added to PEG (10 gram basis) at 20 molar equivalents relative to PEG hydroxyl groups. Reagents were mixed in a round-bottom flask

with a *p*-toluenesulfonic acid catalyst (0.4 mmole; Sigma) and dithiothreitol (0.1 mmole; Sigma) reducing agent. The mixture was refluxed overnight using a Dean-Stark apparatus to remove water produced in the reaction. The contents of the flask were then transferred to a RotoVap to remove the toluene. The final product was precipitated in ice-cold acetone and vacuum filtered. The diester dithiol products were dried overnight under vacuum and stored at −20°C. The reaction proceeded to >95% completion as verified using ^{1}H nuclear magnetic resonance ($CDCl_3$), and thiol content was verified using an Ellman's assay.

Generation of PEG-norbornene microspheres

PEG-norbornene microspheres were generated through a thiolene reaction between PEG-norbornene and either PEG-T-DT, PEG-M-DT, or PEG dithiol (PEG-DT; M_n = 3,400; Laysan Bio). The reaction consisted of an aqueous emulsion previously described [23] between a PEG-rich dispersed phase and a Dextran-rich continuous phase. The PEG-rich phase contained 20 wt.% of four-arm PEG-norbornene, 0.5 molar equivalents of thiol crosslinker (PEG-T-DT, PEG-M-DT, PEG-DT) relative to PEG arms, 0.016 molar equivalents of peptide (VBP or Scramble), and a final concentration of 0.05 wt.% photoinitiator (Irgacure 2959) in DI water. A blank condition was also prepared, using an equivalent amount of DI water in place of the peptide solution. All components of the PEG-rich phase were combined and purged with nitrogen prior to the addition of a 6-fold volumetric excess (relative to PEG phase) of Dextran- rich phase, consisting of 40 wt.% Dextran (M_n = 40,000; Alfa Aesar) in KCl buffer. The PEG- rich phase was emulsified *via* vortexing for one minute in the Dextran phase, and the emulsion was allowed to stabilize for 20 minutes before being exposed to UV light (1.1 J/cm^2) to initiate the polymerization reaction. Impurities and unreacted reagents were removed with a 25-fold dilution in DI water followed by centrifugation at 1600 × g for 5 minutes and two subsequent washes in DI water. The final product was then suspended in DI water, frozen in liquid nitrogen, and lyophilized. Peptide-containing microspheres were suspended in phosphate buffered saline (PBS; Fisher Scientific), and peptide content was verified using either Micro-BCA assay (Thermo Scientific) or by UV-Vis absorbance at 260 nm corresponding to absorbance of tryptophan.

The constraint of microsphere diameter imposed by the capillary tube (6 μm) for injection in the mouse choroidal neovascularization model required the generation of microspheres < 6 μm in diameter. Microsphere emulsification for CNV studies was performed using probe sonication (Branson Sonifier 250) for 40 seconds at 100% duty, and UV polymerization was performed immediately without a stabilization period. Microspheres were washed and characterized as described above. The mean diameter of microspheres was highly dependent on the emulsion conditions (one-way ANOVA p-value < 0.0001), and microspheres generated *via* sonication exhibited a smaller mean diameter (~5 μm) than microspheres generated *via* vortexing (~8 μm) (Fig. 1S).

Characterization of microsphere degradation rate

Microsphere conditions were suspended at 1 mg/mL in PBS and rotated at 37°C. Each day, 10 μL of each microsphere suspension was placed on a microscope slide with 10 μL Trypan Blue (Sigma) stain as previously described by our lab [33]. Microspheres were then imaged

using phase contrast microscopy (Nikon TE300 equipped with 10X objective), and mean microsphere diameter was characterized using ImageJ. This procedure was repeated daily until degradable microspheres (crosslinked with PEG-T-DT and PEG-M-DT) were completely degraded.

Influence of microsphere degradation rate on VEGF sequestering and release

Microspheres were assayed for VEGF sequestering and release as previously described [23,24]. We assessed VEGF binding by incubating microspheres in 10 ng/mL VEGF because of the similar *in vivo* VEGF abundance in wound exudate (~10 ng/mL) and platelet releasate (~1–10 ng/mL). For VEGF sequestering studies, microspheres were incubated in 0.1 wt.% bovine serum albumin (BSA; Fisher) in PBS with 9.9 ng/mL of human recombinant $VEGF_{165}$ (R&D Systems), hereafter referred to as VEGF, and 0.1 ng/mL of [^{125}I]VEGF (Perkin Elmer) for 4 hours at 37°C. Microspheres were subsequently centrifuged at 10,600 × g for 5 minutes, and the supernatant counts per minute (CPM) were measured with a gamma counter (Perkin Elmer) and correlated to VEGF concentration using a standard curve. For release studies, microspheres were pre-loaded with VEGF as above and were incubated in 0.1 wt.% BSA in PBS after washing out un-sequestered VEGF. Microspheres were centrifuged as above, and the supernatants at the specified time points in Figure 2B and Figure 2S were measured on gamma counter and correlated to released VEGF at each time point. VEGF release was measured until the CPM at a given time point was indistinguishable from background.

Impact of VBP microsphere degradation on activity of VEGF

Human umbilical vein endothelial cells (HUVEC; Lonza) were expanded in Medium 199 (CellGro) supplemented with EGM2 and penicillin/streptomycin (Gibco) and were used between passages 6–10. On the day before experiments, HUVECs were plated at 4,000 cells/well in medium containing 2% FBS (Gibco) in Medium 199 in black polystyrene plates pre-coated with Gelatin (Sigma). The next day, microsphere conditions were sanitized by suspension in 70 vol.% ethanol (Fisher) in DI water for at least one hour. Microspheres were washed three times in sterile PBS. For VEGF sequestering experiments, sanitized microspheres were suspended at 1 mg/mL in Medium 199 (M199; CellGro) with 2% FBS serum and either 0 or 10 ng/mL VEGF. For VEGF sustained release experiments, sanitized microspheres were suspended in 0.1 wt.% BSA in PBS with 10 ng/mL VEGF for 45 minutes at 37°C. Microspheres were subsequently centrifuged at 10,600 × g for 5 minutes, and the supernatant was aspirated. Microspheres were then suspended at 1 mg/mL in Medium 199 with 2% FBS. For both VEGF sequestering and sustained VEGF release experiments, culture medium was aspirated from HUVEC-seeded plates, and microsphere suspensions were added to plate at 100 μL per well. HUVECs were incubated with microspheres at 37°C, 95% relative humidity, and 5% CO_2 for 48 hours. At the end of the incubation period, a CellTiter-Blue Cell Viability Assay (Promega) was performed to measure cell metabolic activity by adding 20 μL CellTiter-Blue to each well, incubating for an additional 4 hours, and measuring fluorescence intensity at $590_{excitation}/612_{emission}$. Conditions were assayed in replicates of 6 and compared *via* two-way analysis of variance (ANOVA) and post-hoc Student's t-test ($\alpha = 0.05$), and data are displayed as normalized fluorescence intensity relative to the Blank microsphere condition with each crosslinker type.

Influence of VEGF sequestering and release on VEGF receptor phosphorylation

HUVECs were expanded and used between passages 4–6 for VEGFR2 phosphorylation measurements. Prior to addition to HUVECs, microspheres in VEGF sequestering study (F-VBP, N-VBP, and N-Scramble) were sanitized by exposing to UV for 30 minutes and were incubated at 1 mg/mL in M199 supplemented with 2 vol.% FBS and 10 ng/mL VEGF for 2 days at 37°C. Alternatively, microspheres in VEGF release study (F-VBP, N-VBP, N-Scramble) were sanitized and were incubated at 1 mg/mL in 0.1 wt.% BSA in PBS supplemented with 10 ng/mL VEGF for 4 hours, centrifuged, washed briefly in 2 vol.% FBS in M199, and incubated in 2 vol.% FBS in M199 for 3 days at 37°C. On day 0 of experiments, HUVECs were passaged with trypsin, counted, suspended in M199 with 2 vol. % FBS, and seeded at 20,000 cells/cm^2 in 6 well plates pre-coated with gelatin. On day 1 of experiments, medium was aspirated from each well of 6-well plates and replaced with 1 mL of microsphere suspensions per well (for VEGF sequestering study). Alternately, microspheres in VEGF release study were centrifuged and only the supernatant (termed 'VEGF releasate') from each condition was added to HUVEC culture. HUVECs were incubated with microsphere suspensions (to examine the influence of VEGF sequestering) or VEGF releasate (to examine the influence of released VEGF) for 30 minutes at 37°C. The negative and positive controls consisted of 2 vol.% FBS in M199 without or with 10 ng/mL VEGF supplementation, respectively. Following 30 minute incubation, the wells of each 6-well plate were aspirated and washed with PBS, and 30 μL of 1X Sample Diluent Concentrate 2 (R&D Systems) supplemented with 10 μg/mL Aprotinin (Sigma), 10 μg/mL Leupeptin (Tocris), and 1X HALT Phosphatase Inhibitor (Thermo) was added to each well. HUVECs were subsequently scraped with a cell scraper, and cell lysate was placed in an Eppendorf tube on ice for 15 minutes before storage at −20°C for at least 24 hours. Before assaying, cell lysates were centrifuged at 10,000 × g for 10 minutes at 4°C and stored on ice. Cell lysates were assayed for phosphorylated VEGFR2 using phospho-VEGFR2 ELISA (R&D Systems DYC1766) following standard protocol, using approximately 50 μg of cell lysate per sample per well. The total mass of phosphorylated VEGFR2 in each sample was determined by comparing the optical density (450nm – 540nm) for each sample to a fresh standard curve performed in duplicate. The mass of phosphorylated VEGFR2 in each sample was normalized to total protein content in the cell lysate of each sample, determined using Micro BCA assay following standard procedure using approximately 5 μg of cell lysate per sample per well. Conditions were assayed in triplicate wells, and each well was assayed in duplicate for ELISA and Micro BCA assays.

Generation of elastomeric stencils for endothelial cell sprouting array

Sprouting arrays were generated using an elastomeric stencil as previously described[34]. Polydimethylsiloxane (PDMS; Sylgard 184; Dow Corning) was prepared by mixing the curing agent at 10 vol.% in the base agent. PDMS with curing agent then was dispensed to 15 cm petri dishes (~15 g per dish), degassed for 30 min, and cured for 4 hours at 85°C. 64 wells (arranged in 16 groups of 4 as described below) were stamped out of each hardened PDMS stencil using 3 mm biopsy punch, and stencils were cleaned overnight using a Soxhlet extractor with hexanes. After cleaning, elastomeric stencils were placed at room temperature to remove residual solvent from the extraction and stored in 70 vol.% ethanol in DI water for sanitization before use.

Encapsulating iPSC-ECs in cell-dense sphere

Hydrogel arrays were formed in two steps on subsequent days as previously described[34]. Induced pluripotent stem cell-derived endothelial cells (iPSC-ECs; Cellular Dynamics International, Inc.) were expanded before use in Growth Medium containing 10 vol.% serum supplement (Cellular Dynamics International, Inc.), VEGF LifeFactors kit (LifeLine), penicillin/streptomycin, and VascuLife (LifeLine) and were used at passage 5 for experiments. On day 0 of experiments, iPSC-ECs were encapsulated in eight-arm PEG-norbornene hydrogels containing cell-adhesion peptide (CRGDS; GenScript) and matrix metalloproteinase-degradable crosslinker (KCGGPQGIWGQGCK; GenScript). iPSC-ECs were suspended at 8×10^7 cells/mL in 0.1 wt.% Irgacure 2959 (Ciba) in PBS and immediately diluted 1:1 in a 2X hydrogel precursor solution to make a final solution containing 4 wt.% eight-arm PEG-NB, 2 mM CRGDS, 3.6 mM KCGGPQGIWGQGCK. Cells were then encapsulated by exposing 0.5 μL cell-dense “spheres”, formed at the end of a 10 μL pipet tip, to UV at 0.18 J/cm^2. iPSC-EC cell-dense spheres were cultured overnight in 16 well ProPlate (Grace Bio) slide chambers (with 64-well PDMS stencils installed in place of the 16-well silicone stencil) in Growth Medium at 37°C, 95% relative humidity, and 5% CO_2.

Impact of VEGF sequestering on iPSC-EC sprouting

On day 1 of experiments, iPSC-EC cell-dense spheres were surrounded by a synthetic ECM composed of eight-arm PEG-NB, CRGDS, and KCGGPQGIWGQGCK similarly to above with the addition of microspheres to the outer gel. Medium was aspirated from each well of the 64 well elastomeric stencil, and 10 μL of hydrogel precursor solution, consisting of 4 wt.% eight-arm PEG-NB, 2 mM CRGDS, 3.6 mM KCGGPQGIWGQGCK, 0.05 wt.% Irgacure 2959 in PBS, and 0 or 1 mg/mL of microspheres, was added to each well. Hydrogel arrays were polymerized at 0.09 J/cm^2, after which the 64 well PDMS stencil was replaced by a 16 well silicone stencil (Grace Bio), and medium consisting of 10 vol.% FBS, penicillin/streptomycin, VascuLife, and either 0 or 10 ng/mL VEGF was added to each well. The result of polymerization was four hydrogel posts, each with an encapsulated cell-dense sphere, within each well of the 16-well slide chamber. iPSC-EC arrays were then cultured for 6 days at 37°C, 95% relative humidity, and 5% CO_2 with medium replenished every other day. On day 6 of experiments, cells were stained with 2 μM Calcein-AM and 2 μM Ethidium homodimer-1 for 30 minutes at 37°C. After staining, iPSC-ECs were washed in PBS, fixed, and imaged. We assessed the extent of endothelial sprouting by counting the number of invading Calcein+ cells in the cell-free hydrogel using automated imaging on an epifluorescence microscope (Nikon Ti Eclipse) equipped with 4X objective and filters for phase contrast, TxRed, and FITC. Images were processed using NIS Elements v3.2 (Nikon). Conditions were assayed in replicates of eight and were compared using two-way ANOVA and post-hoc Student’s t-test at $\alpha = 0.05$.

Impact of VEGF sequestering on angiogenesis in mouse choroidal neovascularization model

Microspheres (generated *via* sonication) were sanitized either by washing in 70% ethanol or by exposing to UV for 30 minutes prior to injection. Microspheres (F-VBP, F-Scramble, N-

VBP, and N-Scramble) were suspended at 2 mg/mL in sterile PBS on the day of experiments. Soluble VBP or Scramble peptide (purchased from GenScript) were dissolved, sterile filtered through 0.2 μm filter, and diluted to 20 μg/mL in sterile PBS before experiments. SU4312 (Sigma) was dissolved in DMSO at 5 μg/mL, and Eylea (Regeneron Pharmaceuticals) was dissolved in PBS at 40 μg/mL and sterile filtered through 0.2 μm filter.

The mouse choroidal neovascularization model was generated as previously described (Fig. 6A) [35]. Briefly, C57BL/6J mice (Jackson Laboratories; 6-weeks old female) eyes were dilated using a drop of tropicamide (1%), and mice were anesthetized with ketamine and xylazine. Mice were subjected to photocoagulation (75μm spot size, 0.1s duration, 120mW) at the 3-, 9-, and 12-o'clock positions of the posterior pole of the eye using an OcuLight GL diode laser (Iridex) with a glass coverslip over the eye. Microspheres were injected into each eye (2 μL/eye) using a pump microinjection apparatus (Harvard Apparatus) or Hamilton syringe. Similarly, for experiments with soluble peptide, Soluble VBP or Scramble were injected into each eye (2 μL/eye) using a pump microinjection apparatus. In separate experiments, soluble inhibitors (Vehicle or SU4312) or proteins (IgG or Eylea) were injected into each eye (2 μL/eye) using a pump microinjection apparatus. Mice were allowed to recover for 1 hour and housed for 7 days, whereupon the mice were subjected to a repeat injection of microspheres, soluble peptide, protein, or inhibitor (2 μL/eye). After an additional 7 days of housing, mice were euthanized, and eyes were isolated and fixed in 4 vol. % paraformaldehyde for 2 hours. Eyes were washed three times in PBS, divided at the equator, and the choroid and sclera of the posterior pole were isolated and blocked for 1 hour in 50 vol.% FBS. The isolated tissue (choroid and sclera) were stained with anti-intracellular adhesion molecule-2 (ICAM-2; BD Pharmingen) at 1:500 dilution in 20 vol.% FBS in PBS overnight. The tissues were subsequently washed three times in PBS and stained with secondary antibody. Tissues were washed three times in PBS, mounted with VectaMount AQ (Vector Laboratories), and imaged using epifluorescence microscopy (Zeiss). The area of ICAM-2+ staining (defined as mean CNV area) at each position (3-, 9-, and 12-o'clock) was quantified using ImageJ and automated image thresholding. Outliers were identified and eliminated using the ROUT statistical method [36], and analysis was performed using one-way ANOVA with Tukey's post-hoc test and multiple comparisons correction ($\alpha = 0.05$) in GraphPad Prism.

Results

Microsphere crosslink identity modulates degradation rate

Microspheres crosslinked with ester-containing, dithiol terminated crosslinking groups (Fig. 1A,B) exhibited degradation rates that were variable based on the presence and proximity of ester bonds to terminal thiol groups (Fig. 1C,D). We refer to microspheres crosslinked with PEG-T-DT as F-type microspheres (Fast-degrading), with PEG-M-DT as S-type microspheres (Slowly-degrading), and with PEG-DT as N-type microspheres (Non-degrading). N-type microspheres with no peptide (N-Blank) maintained a constant mean diameter over 18 days (Fig. 1C.v–vi, Fig. 1D). In contrast, S-type microspheres containing no peptide (S-Blank) or containing Scramble peptide (S-Scramble) both exhibited a sharp increase in mean microsphere diameter at day 16 (Fig. 1C.iii–iv) and were completely

degraded in PBS after 18 days (Fig. 1D) or in protein-containing buffer after 12 days (Fig. 2B). F-type microspheres containing no peptide (F-Blank) or containing VBP (F-VBP) both exhibited a sharp increase in mean microsphere diameter at day 1 (Fig. 1C.i–ii) and were completely degraded in PBS after 3 days (Fig. 1D) or in protein-containing buffer after 5 days (Fig. 2B). Microsphere degradation rates were consistent with the degradation rates observed in a previous study with bulk hydrogels crosslinked using the same chemical crosslinking groups [32].

Influence of microsphere degradation rate on VEGF sequestering and release

VBP microspheres sequestered VEGF independent of crosslinker identity, and microsphere degradation rate influenced the release rate of sequestered VEGF. VBP microspheres sequestered significantly more VEGF than Blank and Scramble microspheres regardless of crosslinker identity (Fig. 2A). S-VBP microspheres sequestered significantly more VEGF than either N-VBP or F-VBP microspheres (Fig. 2A), though the interaction between crosslinker and peptide identity was not statistically significant *via* ANOVA. After VEGF sequestering, VBP microspheres released VEGF at a rate that was proportional to the degradation rate of each respective crosslinker (Fig. 2B). S-VBP microspheres exhibited sustained release similar to N-VBP microspheres until day 10, at which point S-VBP microspheres released VEGF rapidly between day 10 and 12 (Fig. 2B). This result is consistent with microsphere degradation data showing complete degradation of S-Type microspheres after approximately two weeks. F-VBP microspheres exhibited more of a “burst” release profile compared to S-VBP and N-VBP microspheres (Fig. 2B), consistent with the fast degradation rate of F-type microspheres. Importantly, the cumulative amount of VEGF released from VBP microspheres was significantly higher than that from Scramble and Blank microspheres (Fig. 2S), reflecting the higher amount of VEGF sequestered to VBP microspheres of all three crosslinker types (Fig. 2A) relative to Scramble and Blank microspheres.

Influence of VBP microsphere degradation on VEGF signaling and activity in HUVEC culture

VBP microspheres reduced VEGF activity in culture upon VEGF sequestering regardless of crosslinker identity (Fig. 3A). Soluble VEGF in the cell culture medium increased HUVEC metabolic activity at 1 and 10 ng/mL relative to the control without VEGF supplementation (Fig. 3S A). Further, 10 ng/mL of supplemented VEGF stimulated VEGFR2 phosphorylation in HUVECs three-fold relative to HUVECs treated with no VEGF (Fig. 4S), and given the similar abundance of VEGF in wound exudate (~10 ng/mL) and platelet releasate (~1–10 ng/mL), 10 ng/mL VEGF was used to determine the influence of VEGF sequestering and release on endothelial cell function *in vitro*. Regardless of crosslinker identity, VBP microspheres reduced HUVEC metabolic activity in culture medium with soluble VEGF (normalized data shown in Fig. 3B). Specifically, F-VBP, S-VBP, and N-VBP microspheres reduced VEGF-dependent HUVEC metabolic activity relative to F-Scramble, S-Scramble, and N-Scramble microspheres, respectively. Both F-VBP and N-VBP microspheres reduced HUVEC metabolic activity relative to F-Blank and N-Blank microspheres, respectively (Fig. 3B). No statistical differences were observed between F-VBP, N-VBP, and S-VBP (Fig. 3B), which suggests that the difference in VEGF

sequestering between these conditions was not biologically-relevant. F-VBP and N-VBP microspheres also reduced the levels of phosphorylated VEGFR2 (pVEGFR2) relative to N-Scramble microspheres in the presence of VEGF (Fig. 3C), which suggests that VBP microspheres reduced VEGF signaling in culture *via* VEGF sequestering and an effective reduction of soluble VEGF available to HUVECs.

In a separate scenario wherein VEGF was pre-loaded into VBP microspheres then added to cell culture, the degradation rate of VBP microspheres significantly influenced the activity of released VEGF (Fig. 4A). N-VBP microspheres preloaded with VEGF increased VEGF-dependent HUVEC metabolic activity upon VEGF release relative to N-Scramble and N-Blank microspheres (normalized data shown in Fig. 4B), which suggests that VEGF released from N-VBP microspheres was active, as previously shown [23,25]. VEGF release from S-VBP microspheres exhibited no effect, as no differences were observed between S-VBP, S-Scramble, or S-Blank microsphere conditions, and the HUVEC metabolic activity upon VEGF release from S-VBP microspheres was significantly lower than from N-VBP microspheres (Fig. 4B). In contrast, VEGF release from F-VBP microspheres decreased VEGF-dependent HUVEC metabolic activity relative to F-Scramble and F-Blank microspheres and relative to S-VBP and N-VBP microspheres (Fig. 4B). The VEGF released from N-VBP microspheres increased the levels of phosphorylated VEGFR2 in cultured HUVECs relative to N-Scramble or F-VBP microspheres, and VEGFR2 phosphorylation upon VEGF release from N-Scramble and F-VBP microspheres was indistinguishable (Fig. 4C). These data together indicate that VEGF released from F-VBP microspheres was less active than that released from controls, S-VBP, or N-VBP microspheres and suggest that F-VBP microspheres reduced the activity of released VEGF.

Influence of VBP microsphere degradation rate on VEGF-dependent EC sprouting in hydrogel arrays

We further investigated the influence of VBP microsphere degradation rate on stem cell-derived endothelial cell sprouting in synthetic hydrogels (Fig. 5A). We examined induced pluripotent stem cell-derived endothelial cell (iPSC-EC) sprouting here due to the well-characterized role of VEGF in promoting iPSC-EC sprouting behavior in hydrogels [37]. VBP microsphere degradation rate influenced the extent of VEGF-dependent iPSC-EC sprouting behavior in PEG-based synthetic hydrogels. In culture medium with supplemented VEGF, encapsulated F-VBP microspheres significantly reduced iPSC-EC sprouting relative to F-Scramble microspheres and the no microsphere (‘-μsphere’) controls (Fig. 5B). Conversely, encapsulated N-VBP microspheres significantly increased iPSC-EC sprouting relative to the ‘-μsphere’ control in culture with VEGF (Fig. 5B). Taken together, F-VBP microspheres reduced VEGFR2 phosphorylation and VEGF activity in culture with endothelial cells, and thus we hypothesized that F-VBP microspheres would reduce neovascularization *in vivo*.

Influence of VEGF sequestering on angiogenesis in mouse choroidal neovascularization model

Injectable, degradable F-VBP microspheres reduced angiogenesis in a murine model of choroidal neovascularization *in vivo*. We defined choroidal neovascularization area as the

area of intracellular adhesion molecule 2 (ICAM-2) staining at each laser photocoagulation spot (Fig. 6A,B). Upon photocoagulation and intravitreal injection to mice, injected F-VBP microspheres reduced the mean choroidal neovascularization (CNV) area relative to F-Scramble microspheres and N-Scramble microspheres. In contrast, N-VBP microspheres did not significantly influence mean CNV area relative to N-Scramble or F-Scramble microspheres (Fig. 6C), indicating that microsphere degradation was critical to angiogenesis inhibition by VBP microspheres. Thus suggests that a combination of VEGF sequestering to, and inactive VEGF release from, F-VBP microspheres led to inhibition of angiogenesis *in vivo*. To gain further insight into the effects of VBP on *in vivo* angiogenesis, we also examined the influence of soluble VBP on CNV area and confirmed that neither soluble Scramble nor soluble VBP reduced CNV area relative to the saline 'Sham' control, though soluble VBP did significantly increase CNV area relative to Sham (Fig. 6D). Finally, we confirmed the ability of F-VBP microspheres to sequester murine VEGF (Fig. 5S), which together suggests that F-VBP microspheres reduced choroidal neovascularization by sequestering and reducing the activity of murine VEGF. The ability of F-VBP microspheres to inhibit angiogenesis in this model was consistent with the effects of two commercial anti-angiogenesis compounds, Eylea and SU5416 (Fig. 6S), which suggests potential therapeutic applications of injectable F-VBP microspheres.

Discussion

Anti-angiogenic therapies typically constitute bolus injections of soluble VEGF-binding antibodies, and these anti-VEGF therapies can reduce angiogenesis in the treatment of age-related macular degeneration [38] and proliferative retinopathy [39]. However, anti-VEGF therapies are limited in their ability to locally regulate VEGF activity, as they readily enter the circulation upon intravitreal injection [40]. In the systemic circulation, the long half-life of anti-VEGF antibodies [41] can increase the risk of long-term systemic effects of anti-VEGF therapy [42]. This motivates the need to develop VEGF-inhibiting therapies whose spatial and temporal activity is tightly controlled. ECM mimicry has previously been used to design growth factor sequestering biomaterials that can locally sequester VEGF [14,43], but these systems are inherently promiscuous for multiple growth factors, and the dynamics of affinity-based growth factor sequestering biomaterials have not been explored in detail.

Here we describe synthetic biomaterials, designed to locally bind VEGF *via* a VEGF-binding peptide. The engineered biomaterials here degraded within a controllable time window *via* hydrolysable crosslinking groups. F-VBP microspheres (exhibiting a fast degradation rate) inhibited angiogenesis *in vivo*, while non-degradable N-VBP microspheres had no effect on angiogenesis *in vivo* (Fig. 6C). An injected solution of VBP did not inhibit angiogenesis, and ultimately increased choroidal neovascularization relative to the sham condition (Fig. 6D), which indicates that tethering of VBP only to degradable microspheres and not to non-degradable microspheres enhanced the ability of VBP to reduce VEGF-dependent neovascularization. These data provide evidence that local VEGF sequestering in the vitreous of the eye is insufficient to reduce choroidal neovascularization, since N-VBP microspheres could sequester VEGF and maintain its activity over time but had no impact on neovascularization in the choroid. Treatment with fast-degrading F-VBP microspheres inhibited choroidal neovascularization, perhaps by release of soluble PEG-VBP conjugates

or release of soluble PEG-VBP-VEGF complexes capable of transporting across the retina and Bruch's membrane and reducing VEGF activity in the neovascular choroidal membrane. The observed inhibition of choroidal neovascularization upon treatment with fast degrading VBP microspheres here is consistent with the inhibition of choroidal neovascularization observed clinically after intraocular delivery of soluble Pegaptanib (VEGF-binding RNA aptamer) [44], Bevacizumab (humanized VEGF-binding antibody) [42], Ranibizumab (chimeric VEGF-binding antibody fragment) [42], and Aflibercept (VEGF-binding fusion protein) [42,45]. In addition, the peptide-based biomaterial approach taken here may overcome the cost and risk of systemic effects of intraocular protein, antibody, or PEG-oligonucleotide delivery [42,46] by virtue of its defined composition and controlled degradation, and thus may present advantages in clinical applications for treatment of pathological angiogenesis that is associated with retinopathy [47] and macular degeneration [48].

The degradation rate of VBP microspheres elicited context-specific effects on EC function *in vitro* and angiogenesis *in vivo*. F-VBP microspheres reduced HUVEC metabolic activity (Fig. 3–4) and reduced iPSC-EC sprouting behavior (Fig. 5B), which suggests that degradable VBP microspheres inhibited multiple EC angiogenic functions relevant to early angiogenesis, in agreement with the influence of F-VBP microspheres on *in vivo* angiogenesis (Fig. 6C). The relative decrease in HUVEC metabolic activity upon VEGF sequestering to F-VBP microspheres (~30% relative to F-Blank microspheres and no VEGF control) compared to the decrease in HUVEC metabolic activity upon VEGF release from F-VBP microspheres (~90% relative to F-Blank and to the no VEGF control) reflects the higher VEGF concentration in the VEGF-sequestering experiment (10 ng/mL) versus the VEGF release experiment, wherein the only source of VEGF was the amount sequestered to the microspheres before addition to culture (~2 ng/mL). Importantly, microspheres in the absence of VEGF did not influence HUVEC metabolic activity *in vitro* (Fig. 3S B), which suggests that the microspheres by themselves did not interfere with the assay or negatively influence cell function. In contrast to F-VBP microspheres that reduced VEGF activity *in vitro* and *in vivo*, N-VBP microspheres exhibited context-dependent effects on *in vitro* EC angiogenic functions and *in vivo* angiogenesis. In the presence of soluble VEGF, N-VBP microspheres reduced HUVEC metabolic activity (Fig. 3B) and reduced VEGFR2 phosphorylation (Fig. 3C) when microspheres were suspended in medium and increased iPSC-EC sprouting when microspheres were encapsulated in hydrogels surrounding iPSC-EC spheres (Fig. 5B). When N-VBP microspheres were pre-loaded with VEGF, they increased HUVEC metabolic activity (Fig. 4B) and stimulated VEGFR2 phosphorylation (Fig. 4C), which suggests that N-VBP microspheres bound to and released VEGF without negatively affecting its activity. We hypothesize that in the iPSC-EC sprouting experiments, the N-VBP microspheres initially sequestered VEGF and served as a "source" for local VEGF release (Fig. 5A). N-VBP microspheres encapsulated in three dimensional hydrogels could also have contributed to the formation of spatial VEGF gradients within the hydrogels [43], which would be expected to promote iPSC-EC chemotaxis and sprouting [49,50]. Future work will be needed to examine this hypothesis by pre-incubating VBP microspheres in VEGF-containing medium and subsequently encapsulating the VEGF-containing microspheres in the sprouting assay to generate a uniform spatial distribution of VEGF

throughout the hydrogel. Our results here with non-degradable VBP microspheres suggest that VEGF-sequestering in hydrogels may promote VEGF activity and increase angiogenesis consistent with the influence of VEGF-sequestering natural or synthetic matrices on VEGF-dependent angiogenic function *in vitro* [17,19] and *in vivo* [15,16].

While several studies have shown that controlled release from biomaterials can potentiate VEGF activity in culture [15,51–55], the hydrogel degradation rate here influenced both the rate of VEGF release and the activity of released VEGF. While the release of VEGF from F-VBP microspheres was faster than from S-VBP or N-VBP microspheres (Fig. 2B), the bioactivity of VEGF released from F-VBP microspheres was lower than the bioactivity of VEGF released from S-VBP or N-VBP microspheres in HUVEC culture (Fig. 4B,C). Controlled release of soluble VBP from F-VBP microspheres and S-VBP microspheres during microsphere degradation would be expected to reduce VEGF activity *in vitro* consistent with the influence of soluble VBP [56], and previous evidence suggests that soluble VBP can compete with microsphere-bound VEGF and reduce the amount of VEGF sequestering to microspheres containing tethered VBP [25]. These data together suggest a mechanism whereby F-VBP microspheres de-activate VEGF during microsphere degradation *via* competitive binding of VEGF to soluble VBP released during microsphere degradation. In contrast to biomaterials that can modulate VEGF release rate and increase VEGF activity [15–17,19,43,57–59], for example through modulating the sulfation of heparin-containing biomaterials[60], or to biomaterials that can control the release of VEGF inhibitors and inhibit VEGF activity [61], here we demonstrated the ability to either potentiate or inhibit VEGF activity by modulating only the biomaterial crosslink identity of biomimetic microspheres. Future work will be necessary to examine the influence of sustained VEGF release and potentiation of VEGF activity in clinical scenarios including limb ischemia in which increased VEGF activity would be hypothesized to promote angiogenesis and improve reperfusion. The modular approach herein may instruct the design of affinity-mediated growth factor binding biomaterials to control the activity of a sequestered growth factor by modulating the degradability of the biomaterial.

Conclusion

VEGF spatial and temporal activity is tightly controlled during wound healing. Unregulated VEGF signaling promotes aberrant angiogenesis that can negatively impact wound healing and contribute to the pathology of diseases including macular degeneration and tumor growth. Growth factor sequestering biomaterials have the ability to spatially regulate growth factor activity by virtue of affinity interactions, but the role of biomaterial degradation has not been explored for spatial and temporal growth factor regulation. Here, we sought to engineer degradable VEGF sequestering hydrogel microspheres to provide a mechanism for temporally-controlled VEGF regulation. We observed that the degradation rate of VEGF-sequestering hydrogel microspheres strongly influenced the biological activity of VEGF in endothelial cell culture, and only VEGF-sequestering microspheres with inherent degradability reduced VEGF-dependent cell function and VEGFR2 activation *in vitro* and angiogenesis *in vivo*. These results highlight the ability to control growth factor activity in affinity-based biomaterials through modulating biomaterial degradability and demonstrate a

potential therapeutic application of injectable, degradable VEGF-binding microspheres to reduce pathological angiogenesis *in vivo.*

Supplementary Material

Refer to Web version on PubMed Central for supplementary material.

Acknowledgments

The authors acknowledge support from the National Institutes of Health (T32 HL007936-12, RO1 HL093282, R21 EB016381, R01 EY022883, P30 EY016665, and T32 HL110853), the Environmental Protection Agency (#835737), Retina Research Foundation, and Research to Prevent Blindness.

References Cited

1. Silva EA, Mooney DJ. Spatiotemporal control of vascular endothelial growth factor delivery from injectable hydrogels enhances angiogenesis. J Thromb Haemost. 2007; 5:590–8. [PubMed: 17229044]
2. von Degenfeld G, Banfi A, Springer ML, Wagner RA, Jacobi J, Ozawa CR, et al. Microenvironmental VEGF distribution is critical for stable and functional vessel growth in ischemia. FASEB J. 2006; 20:2657–9. [PubMed: 17095533]
3. Ozawa CR, Banfi A, Glazer NL, Thurston G, Springer ML, Kraft PE, et al. Microenvironmental VEGF concentration , not total dose , determines a threshold between normal and aberrant angiogenesis. J Clin Invest. 2004; 113:516–527. [PubMed: 14966561]
4. Lee RJ, Springer ML, Blanco-Bose WE, Shaw R, Ursell PC, Blau HM. VEGF Gene Delivery to Myocardium : Deleterious Effects of Unregulated Expression. Circulation. 2000; 102:898–901. [PubMed: 10952959]
5. Springer ML, Chen AS, Kraft PE, Bednarski M, Blau HM. VEGF gene delivery to muscle: potential role for vasculogenesis in adults. Mol Cell. 1998; 2:549–558. [PubMed: 9844628]
6. Sahin H, Tholema N, Petersen W, Raschke MJ, Stange R. Impaired Biomechanical Properties Correlate with Neoangiogenesis as well as VEGF and MMP-3 Expression during Rat Patellar Tendon Healing. 2012:1952–1957.
7. Hou Y, Mao Z, Wei X, Lin L, Chen L, Wang H, et al. Effects of transforming growth factor-beta1 and vascular endothelial growth factor 165 gene transfer on Achilles tendon healing. Matrix Biol. 2009; 28:324–335. [PubMed: 19389474]
8. Tille JC, Pepper MS. Hereditary vascular anomalies: new insights into their pathogenesis. Arterioscler Thromb Vasc Biol. 2004; 24:1578–90. [PubMed: 15231518]
9. Plate KH, Breier G, Weich HA, Risau W. Vascular endothelial growth factor is a potential tumour angiogenesis factor in human gliomas in vivo. Nature. 1992; 359:845–848. [PubMed: 1279432]
10. Lip PL, Belgore F, Blann AD, Hope-Ross MW, Gibson JM, Lip GY. Plasma VEGF and soluble VEGF receptor FLT-1 in proliferative retinopathy: relationship to endothelial dysfunction and laser treatment. Invest Ophthalmol Vis Sci. 2000; 41:2115–9. [PubMed: 10892852]
11. Nowak JZ. Age-related macular degeneration (AMD): pathogenesis and therapy. Pharmacol Rep. 2006; 58:353–63. [PubMed: 16845209]
12. Senger DR, Perruzzi CA, Feder J, Dvorak HF. A highly conserved vascular permeability factor secreted by a variety of human and rodent tumor cell lines. Cancer Res. 1986; 46:5629–5632. [PubMed: 3756910]
13. Wade RJ, Burdick JA. Engineering ECM signals into biomaterials. Mater Today. 2012; 15:454–459.
14. Hudalla GA, Murphy WL. Biomaterials that regulate growth factor activity via bioinspired interactions. Adv Funct Mater. 2011; 21:1754–1768. [PubMed: 21921999]

15. Chow LW, Bitton R, Webber MJ, Carvajal D, Shull KR, Sharma AK, et al. A bioactive self-assembled membrane to promote angiogenesis. Biomaterials. 2011; 32:1574–82. [PubMed: 21093042]
16. Mammadov R, Mammadov B, Toksoz S, Aydin B, Yagci R, Tekinay AB, et al. Heparin mimetic peptide nanofibers promote angiogenesis. Biomacromolecules. 2011; 12:3508–19. [PubMed: 21853983]
17. Chow LW, Wang L, Kaufman DB, Stupp SI. Self-assembling nanostructures to deliver angiogenic factors to pancreatic islets. Biomaterials. 2010; 31:6154–6161. [PubMed: 20552727]
18. Guo H, Cui G, Yang J, Wang C, Zhu J, Zhang L, et al. Sustained delivery of {VEGF} from designer self-assembling peptides improves cardiac function after myocardial infarction. Biochem Biophys Res Commun. 2012; 424:105–111. [PubMed: 22732415]
19. Martino MM, Tortelli F, Mochizuki M, Traub S, Ben-David D, Kuhn GAS, et al. Engineering the growth factor microenvironment with fibronectin domains to promote wound and bone tissue healing. Sci Transl Med. 2011; 3:100ra89.
20. Martino MM, Hubbell JSA. The 12th-14th type III repeats of fibronectin function as a highly promiscuous growth factor-binding domain. FASEB J. 2010; 24:4711–21. [PubMed: 20671107]
21. Mosesson MW. Fibrinogen and fibrin structure and functions. J Thromb Haemost. 2005; 3:1894–1904. [PubMed: 16102057]
22. Capila I, Linhardt RJ. Heparin-protein interactions. Angew Chemie. 2002; 41:391–412.
23. Belair DG, Khalil AS, Miller MJ, Murphy WL. Serum-Dependence of Affinity-Mediated VEGF Release from Biomimetic Microspheres. Biomacromolecules. 2014; 15:2038–2048. [PubMed: 24773176]
24. Belair DG, Murphy WL. Specific VEGF Sequestering to Biomaterials : Influence of Serum Stability. Acta Biomater. 2013; 9:8823–8831. [PubMed: 23816648]
25. Impellitteri NA, Toepke MW, Lan Levengood SK, Murphy WL. Specific VEGF sequestering and release using peptide-functionalized hydrogel microspheres. Biomaterials. 2012; 33:3475–84. [PubMed: 22322198]
26. Toepke MW, Impellitteri NA, Lan Levengood SK, Boeldt DS, Bird IM, Murphy WL. Regulating Specific Growth Factor Signaling Using Immobilized Branched Ligands. Adv Healthc Mater. 2012; 1:457–460. [PubMed: 23184776]
27. Bao P, Kodra A, Tomic-Canic M, Golinko MS, Ehrlich HP, Brem H. The role of vascular endothelial growth factor in wound healing. J Surg Res. 2009; 153:347–58. [PubMed: 19027922]
28. Nissen NN, Polverini PJ, Koch AE, Volin MV, Gamelli RL, Dipietro LA. Vascular Endothelial Growth Factor Mediates Angiogenic Activity during the Proliferative Phase of Wound Healing. Am J Pathol. 1998; 152:1445–1452. [PubMed: 9626049]
29. Langer R, Tirrell DA. Designing materials for biology and medicine. Nature. 2004; 428:487–92. [PubMed: 15057821]
30. Holzapfel BM, Reichert JC, Schantz JT, Gbureck U, Rackwitz L, Nöth U, et al. How smart do biomaterials need to be? A translational science and clinical point of view. Adv Drug Deliv Rev. 2013; 65:581–603. [PubMed: 22820527]
31. Fairbanks BD, Schwartz MP, Halevi AE, Nuttelman CR, Bowman CN, Anseth KS. A Versatile Synthetic Extracellular Matrix Mimic via Thiol-Norbornene Photopolymerization. Adv Mater. 2009; 21:5005–5010. [PubMed: 25377720]
32. Zustiak SP, Leach JB. Hydrolytically degradable poly(ethylene glycol) hydrogel scaffolds with tunable degradation and mechanical properties. Biomacromolecules. 2011; 11:1348–1357. [PubMed: 20355705]
33. Parlato M, Johnson A, Hudalla GA, Murphy WL. Adaptable poly(ethylene glycol) microspheres capable of mixed-mode degradation. Acta Biomater. 2013; 9:9270–80. [PubMed: 23958780]
34. Belair DG, Schwartz MP, Knudsen TB, Murphy WL. Human iPSC-Derived Endothelial Cell Sprouting Assay in Synthetic Hydrogel Arrays. 2016 Submitted.
35. Wang S, Sorenson CM, Sheibani N. Lack of thrombospondin 1 and exacerbation of choroidal neovascularization. Arch Ophthalmol. 2012; 130:615–20. [PubMed: 22232368]
36. Motulsky HJ, Brown RE. Detecting outliers when fitting data with nonlinear regression – a new method based on robust nonlinear regression and the false discovery rate. 2006; 20:1–20.

37. Belair DG, Whisler JA, Valdez J, Velazquez J, Molenda JA, Vickerman V, et al. Human Vascular Tissue Models Formed from Human Induced Pluripotent Stem Cell Derived Endothelial Cells. Stem Cell Rev. 2014
38. Ferrara N. Vascular endothelial growth factor and age-related macular degeneration : from basic science to therapy. Nat Med. 2010; 16:xix–xxiii.
39. Abdallah W, Fawzi AA. Anti-VEGF therapy in proliferative diabetic retinopathy. Int Ophthalmol Clin. 2009; 49:95–107. [PubMed: 19349790]
40. Zhu Q, Ziemssen F, Henke-Fahle S, Tatar O, Szurman P, Aisenbrey S, et al. Vitreous Levels of Bevacizumab and Vascular Endothelial Growth Factor-A in Patients with Choroidal Neovascularization. Ophthalmology. 2008; 115:1750–1756. [PubMed: 18708261]
41. Zalevsky J, Chamberlain AK, Horton HM, Karki S, Leung IW, Sproule TJ, et al. Enhanced antibody half-life improves in vivo activity. Nat Biotechnol. 2010; 28:157–159. [PubMed: 20081867]
42. Keane PA, Sadda SR. Development of Anti-VEGF Therapies for Intraocular Use: A Guide for Clinicians. J Ophthalmol. 2012; 2012
43. Belair DG, Le NN, Murphy WL. Design of growth factor sequestering biomaterials. Chem Commun. 2014
44. Ng EWM, Shima DT, Calias P, Cunningham ET, Guyer DR, Adamis AP. Pegaptanib, a targeted anti-VEGF aptamer for ocular vascular disease. Nat Rev Drug Discov. 2006; 5:123–32. [PubMed: 16518379]
45. Saishin Y, Saishin Y, Takahashi K, Lima e Silva R, Hylton D, Rudge JS, et al. VEGF-TRAP(R1R2) suppresses choroidal neovascularization and VEGF-induced breakdown of the blood-retinal barrier. J Cell Physiol. 2003; 195:241–8. [PubMed: 12652651]
46. D'Andrea LD, Del Gatto A, Pedone C, Benedetti E. Peptide-based molecules in angiogenesis. Chem Biol Drug Des. 2006; 67:115–26. [PubMed: 16492159]
47. Aiello LP, Avery RL, Arrigg PG, Keyt BA, Jampel HD, Shah ST, et al. Vascular Endothelial Growth Factor in Ocular Fluid of Patients with Diabetic Retinopathy and other Retinal Disorders. N Engl J Med. 1994; 331:1480–1487. [PubMed: 7526212]
48. Lopez PF, Sippy BD, Michael Lambert H, Thach AB, Hinton DR. Transdifferentiated retinal pigment epithelial cells are immunoreactive for vascular endothelial growth factor in surgically excised age-related macular degeneration-related choroidal neovascular membranes. Investig Ophthalmol Vis Sci. 1996; 37:855–868. [PubMed: 8603870]
49. Gerhardt H, Golding M, Fruttiger M, Ruhrberg C, Lundkvist A, Abramsson A, et al. VEGF guides angiogenic sprouting utilizing endothelial tip cell filopodia. J Cell Biol. 2003; 161:1163–77. [PubMed: 12810700]
50. Akeson A, Herman A, Wiginton D, Greenberg J. Endothelial cell activation in a VEGF-A gradient: relevance to cell fate decisions. Microvasc Res. 2010; 80:65–74. [PubMed: 20144626]
51. Tae G, Scatena M, Stayton PS, Hoffman AS, Allan S. PEG-cross-linked heparin is an affinity hydrogel for sustained release of vascular endothelial growth factor. J Biomater Sci. 2006; 17:187–97.
52. Jay SM, Saltzman WM. Controlled delivery of VEGF via modulation of alginate microparticle ionic crosslinking. J Control Release. 2009; 134:26–34. [PubMed: 19027807]
53. Hall H. Modified fibrin hydrogel matrices: both, 3D-scaffolds and local and controlled release systems to stimulate angiogenesis. Curr Pharm Des. 2007; 13:3597–607. [PubMed: 18220797]
54. Formiga FR, Pelacho B, Garbayo E, Abizanda G, Gavira JJ, Simon-Yarza T, et al. Sustained release of VEGF through PLGA microparticles improves vasculogenesis and tissue remodeling in an acute myocardial ischemia-reperfusion model. J Control Release. 2010; 147:30–7. [PubMed: 20643169]
55. Zisch AH, Lutolf MP, Ehrbar M, Raeber GP, Rizzi SC, Davies N, et al. Cell-demanded release of VEGF from synthetic, biointegrative cell ingrowth matrices for vascularized tissue growth. FASEB J. 2003; 17:2260–2. [PubMed: 14563693]
56. Germeroth L, Piossek C, Thierauch KH, Schneider-Mergener J, Volkmer-Engert R, Bachmann MF, et al. Potent inhibition of angiogenesis by D,L-peptides derived from vascular endothelial growth factor receptor 2. Thromb Haemost. 2003:501–510. [PubMed: 12958620]

57. des Rieux A, Ucakar B, Mupendwa BPK, Colau D, Feron O, Carmeliet P, et al. 3D systems delivering VEGF to promote angiogenesis for tissue engineering. J Control Release. 2011; 150:272–8. [PubMed: 21130820]

58. Zisch AH, Lutolf MP, Hubbell JSA. Biopolymeric delivery matrices for angiogenic growth factors. Cardiovasc Pathol. 2003; 12:295–310. [PubMed: 14630296]

59. Vulic K, Shoichet MS. Tunable growth factor delivery from injectable hydrogels for tissue engineering. J Am Chem Soc. 2012; 134:882–5. [PubMed: 22201513]

60. Freudenberg U, Zieris A, Chwalek K, Tsurkan MV, Maitz MF, Atallah P, et al. Heparin desulfation modulates VEGF release and angiogenesis in diabetic wounds. J Control Release. 2015; 220(Part A):79–88. [PubMed: 26478015]

61. Langer R, Murray J. Angiogenesis inhibitors and their delivery systems. Appl Biochem Biotechnol. n.d; 8:9–24. [PubMed: 6206793]

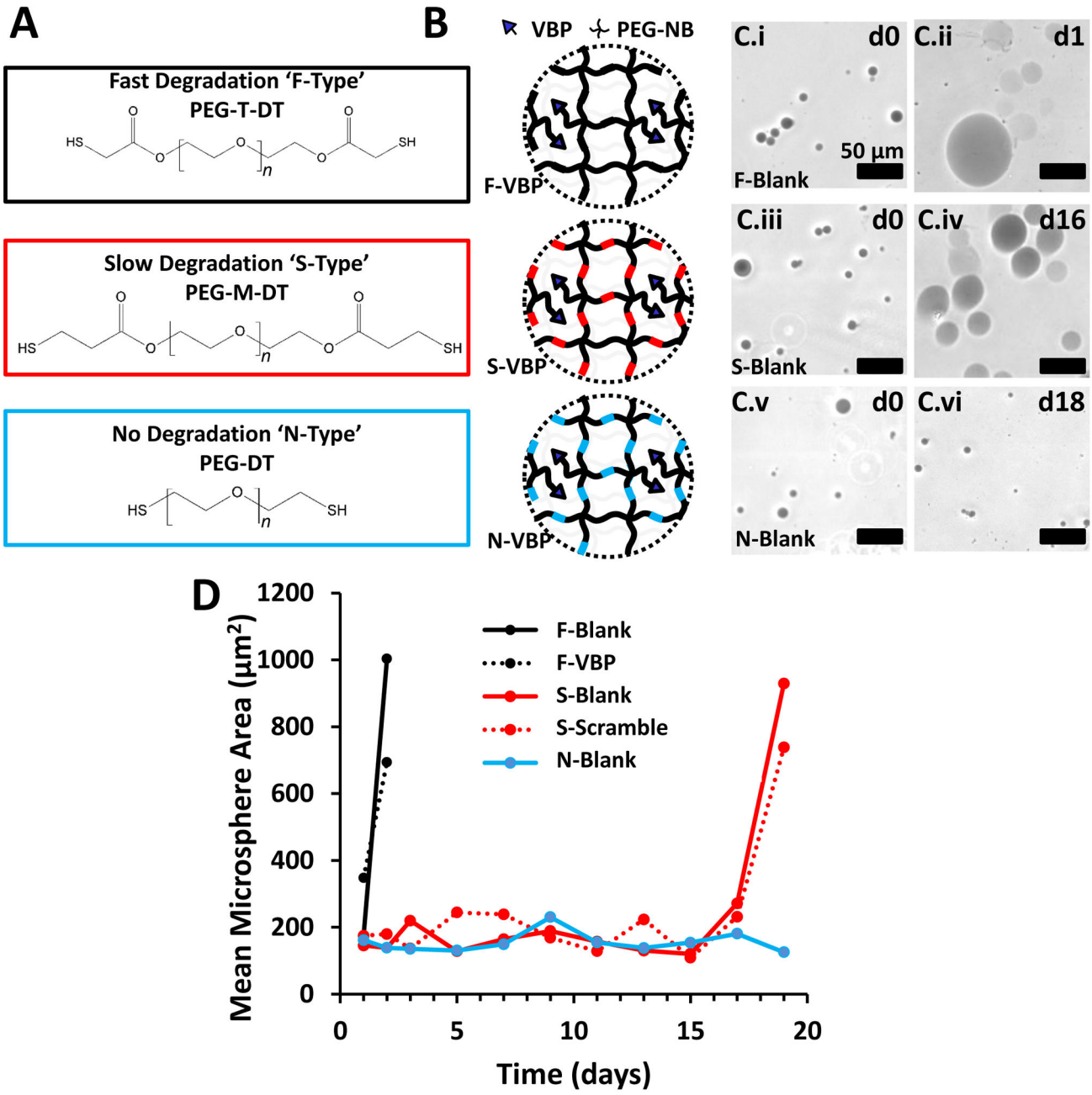

Figure 1.

Influence of chemical crosslinker identity on PEG microsphere degradation rate. A: Chemical structure of PEG-T-DT, PEG-M-DT, and PEG-DT. The molecular weight of each PEG chain is 3.4 kDa, thus the number of repeat ethylene glycol units, 'n', in each schematic is approximately 77. B: Schematic of VBP microspheres crosslinked with fast-degrading PEG-T-DT crosslinker (F-Type), slow-degrading PEG-M-DT crosslinker (S-Type), and non-degrading PEG-DT (N-Type). C: Phase contrast images of Trypan-stained Blank F-Type microspheres at day 0 (C.i) and day 1 (C.ii), S-Type microspheres at day 0 (C.iii) and day 16 (C.iv), and N-Type microspheres at day 0 (C.v) and day 18 (C.vi). Scale

bar represents 50 μm. D: Line graph represents mean microsphere area (μm^2) over time for F-Blank (Black), S-Blank (Red), and N-Blank (Blue) microspheres. Peptide-containing microspheres are represented for F-VBP microspheres (Dashed Black) and S-Scramble microspheres (Dashed Red). F-Scramble, S-VBP, N-VBP, and N-Scramble were omitted for brevity, as the degradation profiles for microspheres of each crosslinker type was independent of the presence of peptide.

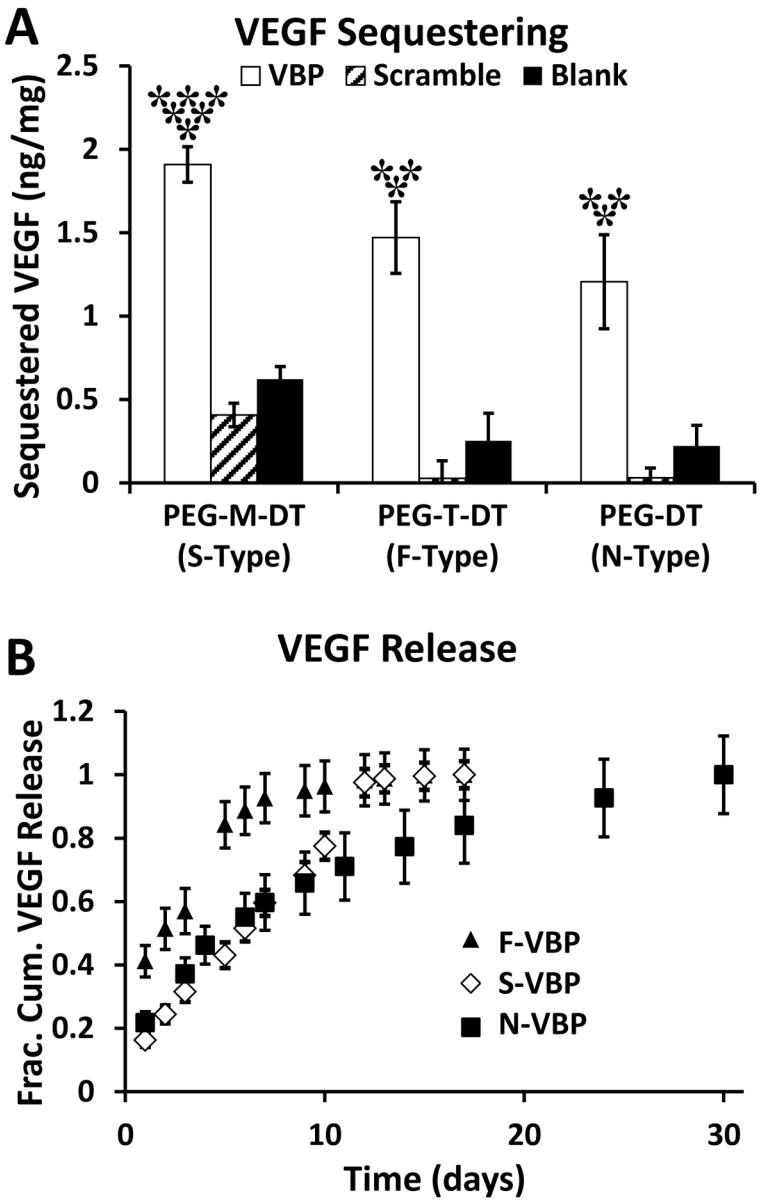

Figure 2.

VBP microspheres sequestered VEGF, and VEGF release rate was dependent on crosslinker identity. A: Sequestered VEGF (ng VEGF per mg microspheres) to microspheres containing peptide (VBP, Scramble) or no peptide (Blank) and varying crosslinker identities (PEG-M-DT, PEG-T-DT, and PEG-DT). Two-way analysis of variance was performed (microsphere peptide identity p-value< 0.0001, microsphere crosslink type p-value< 0.0001, interaction p-value> 0.05) with post-hoc Student's t-test. Statistical significance relative to Scramble (**) and Blank (*) microspheres for each crosslinker type or relative to F-VBP and N-VBP (***) is denoted for $\alpha = 0.05$ using post-hoc Tukey's test. B: VEGF release curves presented as fractional cumulative VEGF release (normalized to the final time point). A,B: Data represent mean + /− standard deviation for three replicates per condition.

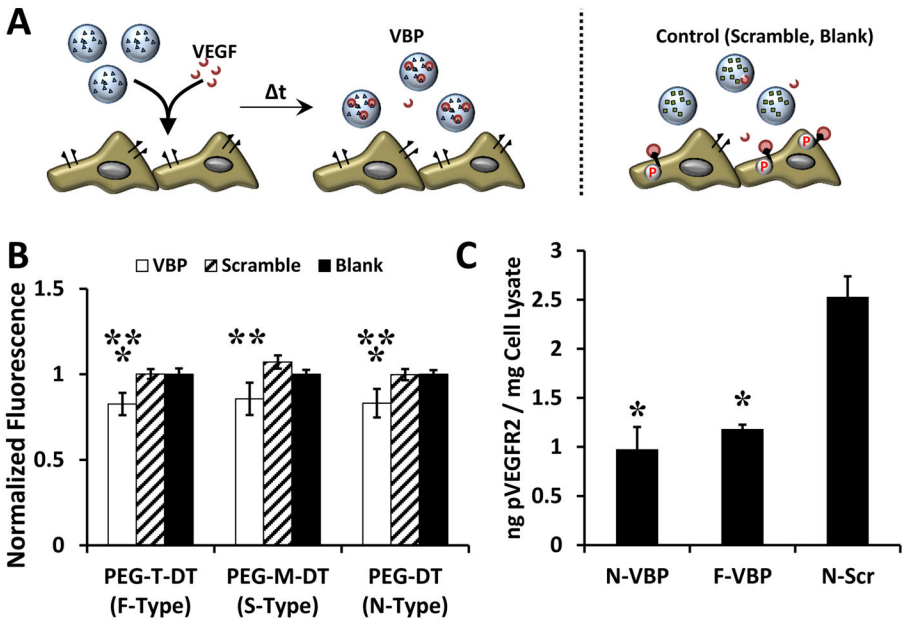

Figure 3.

VBP microspheres reduced VEGF-dependent metabolic activity and VEGFR activation in HUVEC culture A: Schematic of the VEGF sequestering by VBP microspheres (or Scramble or Blank microspheres) in HUVEC culture containing VEGF. B: Relative HUVEC metabolic activity (given as normalized fluorescence intensity of each condition relative to the Blank microsphere condition of each crosslinker type) upon addition of VEGF-containing medium to Blank microspheres (containing no peptide), VBP, or Scramble and varying crosslinker identity. Two-way analysis of variance was performed (microsphere peptide identity p-value< 0.0001, microsphere crosslink type p-value> 0.05, interaction p-value> 0.05) with post-hoc Student's t-test. Statistical significance is denoted compared to Scramble (**) and Blank (*) microspheres at each respective crosslinker type or between conditions in brackets for p-value < 0.05 using Student's t-test. Error bars represent the standard deviation about the mean for six replicates per condition. C: Amount of phosphorylated VEGFR2 (in ng) measured *via* ELISA normalized to the total protein content of the cell lysate (in mg) after treatment of HUVECs with microsphere supernatants from microspheres (F-VBP, N-VBP, or N-Scramble) that were pre-incubated in 10 ng/mL VEGF for 2 days in culture medium containing 2 vol.% FBS in M199. Data is presented as mean + /− standard deviation for three replicates per condition, and statistical significance is denoted relative to N-Scramble control at p-value < 0.05 (*) using one-way ANOVA and Tukey's post-hoc test.

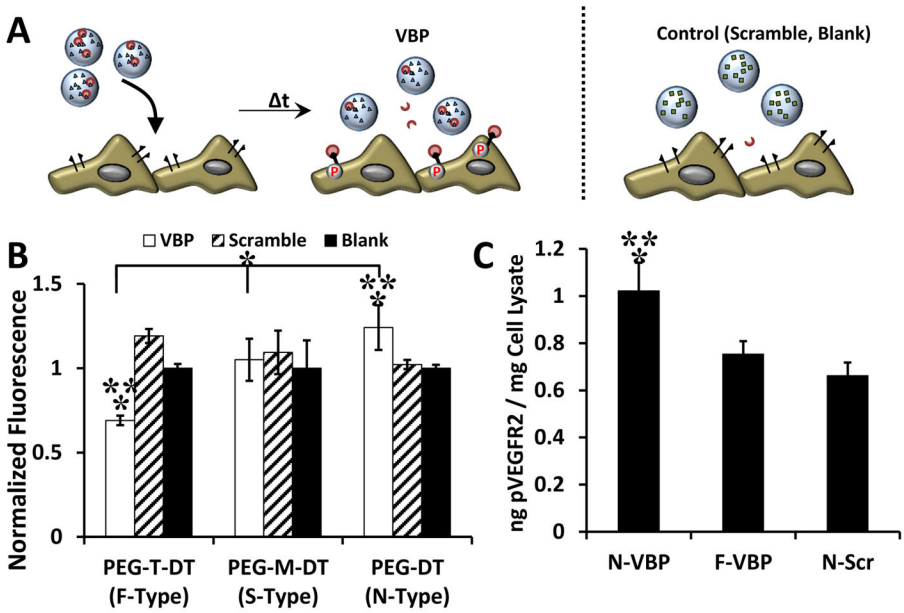

Figure 4.

VBP microspheres exhibited different effect on HUVEC metabolic activity upon VEGF release depending on crosslink identity. A: Schematic of the hypothesized impact of VEGF release from VBP microspheres (or from Scramble or Blank microspheres) in HUVEC culture. B: Relative HUVEC metabolic activity (given as normalized fluorescence intensity of each condition relative to the Blank microsphere condition of each crosslinker type) upon addition of Blank, VBP, or Scramble microspheres (with different crosslinker identity) that were pre-incubated in VEGF, briefly washed, and delivered to HUVEC culture. Two-way analysis of variance was performed (microsphere peptide identity p-value< 0.0001, microsphere crosslink type p-value< 0.0001, interaction p-value< 0.0001) with post-hoc Student's t-test. Statistical significance is denoted compared to Scramble (**) and Blank (*) microspheres at each respective crosslinker type or between conditions in brackets at p-value < 0.05 using Student's t-test. Data represent mean + /− standard deviation for six replicates per condition. C: Amount of phosphorylated VEGFR2 (in ng) measured *via* ELISA normalized to the total protein content of the cell lysate (in mg) after treatment of HUVECs with VEGF releasate from microspheres (F-VBP, N-VBP, or N-Scramble) after pre-incubation with 10 ng/mL VEGF, a brief wash, and 3 days of release into culture medium containing 2 vol.% FBS in M199. Data is presented as mean + /− standard deviation for three replicates per condition, and statistical significance is denoted relative to N-Scramble control (*) or F-VBP (**) at p-value < 0.05 (*) using one-way ANOVA with Tukey's post-hoc test.

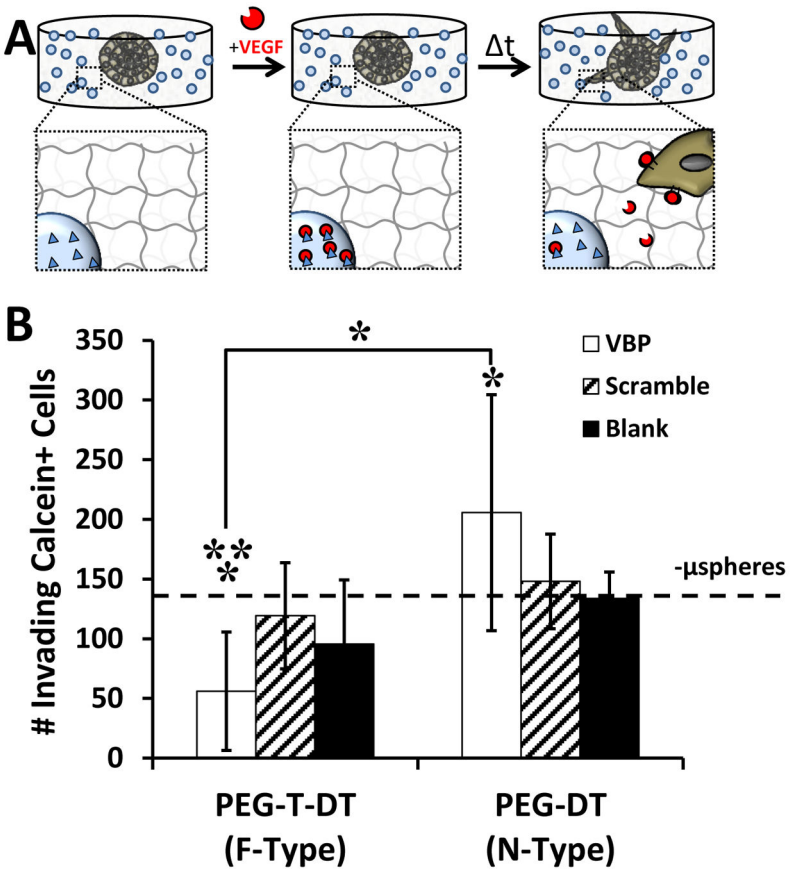

Figure 5.

Influence of VBP microspheres on iPSC-EC sprouting behavior in hydrogels. A:Schematic demonstrating iPSC-EC sprouting away from cell-dense sphere into surrounding synthetic hydrogel with encapsulated VBP microspheres. B: iPSC-EC sprouting quantified as the number of invading Calcein+ cells for each condition. Condition with no microspheres (-μspheres) in the presence of VEGF is shown with a dashed line. Two-way analysis of variance was performed (microsphere peptide identity p-value> 0.05, microsphere crosslink type p-value= 0.002, interaction p-value= 0.016) with post-hoc Student's t-test. Statistical significance for Student's t-test denoted compared to Scramble (**) and no microsphere (*) conditions or between conditions in brackets at $\alpha = 0.05$). Data is presented as mean + /− standard deviation for eight replicates per condition

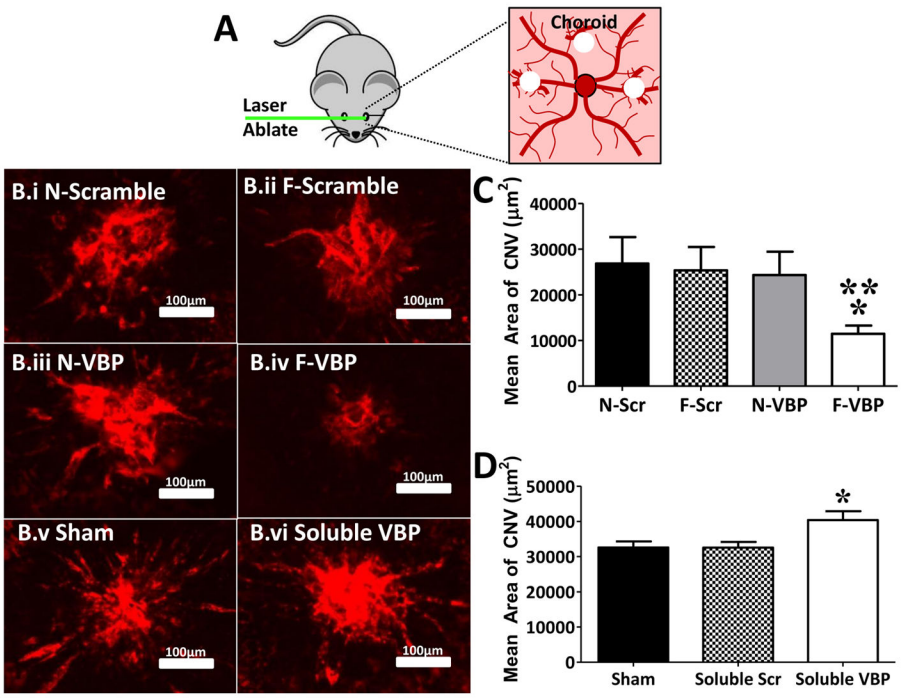

Figure 6.

Degradable VBP microspheres reduced neovascularization in a mouse choroidal neovascularization model. A: Schematic of laser ablation of the mouse choroid in murine CNV model. Laser ablation was performed at the 3-, 9-, and 12-o'clock positions on the posterior of the eye. B: Representative fluorescent micrographs of ICAM2+ vessels in mouse CNV model after treatment with N-Scramble (B.i), F-Scramble (B.ii), N-VBP (B.iii), or F-VBP microspheres (B.iv), or sham (saline, B.v) or Soluble VBP (B.vi). C: Mean CNV area in μm^2 (defined as the area of ICAM2+ vasculature in the choroid) after treatment with either N-Scramble (N-Scr), F-Scramble (F-Scr), N-VBP, or F-VBP microspheres. Data were aggregated for two independent experiments, and error bars represent standard error about the mean (SEM) for 6 (N-Scramble), 5 (F-Scramble), 7 (N-VBP), and 14 mice (F-VBP). Statistical significance was determined using one-way analysis of variance with Tukey's post-hoc test and a Tukey multiple comparisons correction and is denoted for p-value < 0.05 relative to N-Scramble (**) or F-Scramble (*) microspheres. D: Mean CNV area (μm^2) after treatment with saline (Sham), 20 μg/mL Soluble Scramble, or 20 μg/mL Soluble VBP. Error bars represent SEM for 8 mice per condition. Statistical significance was determined using one-way analysis of variance with Tukey's post-hoc test and Tukey multiple comparisons correction and is denoted (*) for p-value < 0.05 relative to Sham.